HHS Public Access

Author manuscript

JACC Cardiovasc Imaging. Author manuscript; available in PMC 2015 December 29.

Published in final edited form as:

JACC Cardiovasc Imaging. 2008 November ; 1(6): 705–717. doi:10.1016/j.jcmg.2008.06.008.

Characterization and Quantification of Vortex Flow in the Human Left Ventricle by Contrast Echocardiography Using Vector Particle Image Velocimetry

Geu-Ru Hong, MD, PhD[*,†], **Gianni Pedrizzetti, PhD**[‡], **Giovanni Tonti, MD**[§], **Peng Li, MD, PhD**[*], **Zhao Wei, MD, PhD**[*], **Jin Kyung Kim, MD, PhD**[‖], **Abinav Baweja**[‖], **Shizhen Liu, MD, PhD**[*], **Namsik Chung, MD, PhD**[¶], **Helene Houle, RDCS**[#], **Jagat Narula, MD, PhD, FACC**[‖], and **Mani A. Vannan, MBBS, FACC**[*]

[*]Ohio State University, Columbus, Ohio

[†]Yeungnam University, Daegu, Korea

[‡]University of Trieste, Trieste, Italy

[§]Catholic University of Sacred Heart of Campobasso, Campobasso, Italy

[‖]University of California, Irvine, Irvine, California

[¶]Yonsei University, Seoul, Korea

[#]Siemens Medical Solutions, Mountain View, California.

Abstract

OBJECTIVES—The aims of this study were to: 1) assess the feasibility of left ventricular (LV) vortex flow analysis using contrast echocardiography (CE); and 2) characterize and quantify LV vortex flow in normal subjects and patients with LV systolic dysfunction.

BACKGROUND—Vortices that form during LV filling have specific geometry and anatomical locations that are critical determinants of directed blood flow during ejection. Therefore, it is clinically relevant to assess the vortex flow patterns to better understand the LV function.

METHODS—Twenty-five patients (10 normal and 15 patients with abnormal LV systolic function) underwent CE with intravenous contrast agent, Definity (Bristol-Myers Squibb Medical Imaging, Inc., North Billerica, Massachusetts). The velocity vector and vorticity were estimated by particle image velocimetry. Average vortex parameters including vortex depth, transverse position, length, width, and sphericity index were measured. Vortex pulsatility parameters including relative strength, vortex relative strength, and vortex pulsation correlation were also estimated.

Reprint requests and correspondence: Dr. Mani A. Vannan, Division of Cardiovascular Medicine, OSUMC, 473 West 12th Avenue, DHLRI Suite 200, Columbus, Ohio 43210. *mvannan@osumc.edu*..

APPENDIX

For accompanying videos and video legends, and the quantification of vortex flow from particle image velocimetry, please see the online version of this article.

RESULTS—Vortex depth and vortex length were significantly lower in the abnormal LV function group (0.443 ± 0.04 vs. 0.482 ± 0.06, $p < 0.05$; 0.366 ± 0.06 vs. 0.467 ± 0.05, $p < 0.01$, respectively). Vortex width was greater (0.209 ± 0.05 vs. 0.128 ± 0.06, $p < 0.01$) and sphericity index was lower (1.86 ± 0.5 vs. 3.66 ± 0.6, $p < 0.001$) in the abnormal LV function group. Relative strength (1.13 ± 0.4 vs. 2.10 ± 0.8, $p < 0.001$), vortex relative strength (0.57 ± 0.2 vs. 1.19 ± 0.5, $p < 0.001$), and vortex pulsation correlation (0.63 ± 0.2 vs. 1.31 ± 0.5, $p < 0.001$) were significantly lower in the abnormal LV function group.

CONCLUSIONS—It was feasible to quantify LV vorticity arrangement by CE using particle image velocimetry in normal subjects and those with LV systolic dysfunction, and the vorticity imaging by CE may serve as a novel approach to depict vortex, the principal quantity to assess the flow structure.

Keywords

vortex; contrast echocardiography; particle image velocimetry

A vortex can be described as a fluid structure that possesses circular or swirling motion. Therefore, vorticity (the curl of the velocity field) represents the skeleton of the flow field and the principal quantity to define the flow structure (1,2). Intraventricular blood flow is optimized to facilitate efficient systolic ejection of blood. Vortices that form during left ventricular (LV) filling have specific geometry and anatomical location that are critical determinants of directed blood flow during ejection (1,3). The formation of abnormal vortices also relates to the underlying fluid dynamics in LV dysfunction (4,5). Therefore, vortex flow may offer a novel index of LV dysfunction not available in conventional indexes and may be of incremental value.

Direct measurement of vortices requires techniques that provide 3-dimensional flow information. Several studies using magnetic resonance imaging (MRI) have demonstrated that vortex in the heart might prevent collision of flow, avoid excessive dissipation of energy, redirect and sling blood towards left ventricular outflow tract (LVOT), and enhance reciprocation of atrial and ventricular function (1,3,6). Vorticity imaging by contrast echocardiography (CE) using velocity vector profiles is a novel approach to study the LV vortex. We hypothesized that changes in the LV vortex flow pattern may correlate closely with LV function and that assessment of LV function using LV vortex flow analysis affords more accurate prediction of the patient's hemodynamic status. Therefore, the aims of this study were: 1) to assess the feasibility of LV vortex flow analysis using CE; and 2) to characterize and quantify LV vortex flow in normal subjects and patients with LV systolic dysfunction.

METHODS

Study population

A total of 25 subjects were prospectively enrolled in this study; 10 normal control subjects (age 52 ± 18 years) and 15 patients with LV dysfunction (age 51 ± 11 years). The abnormal LV function group was comprised of patients who have reduced LV systolic function (ejection fraction <40%) at baseline echocardiography. Patients with significant atrial or

ventricular arrhythmia, significant valvular disease (of greater than moderate severity), or inability to obtain adequate echocardiographic examination were also excluded. The study was approved by the Institutional Review Board of the University of California, Irvine, and a written informed consent was obtained from all patients.

Two-dimensional (2D) and CE

All patients underwent 2D and Doppler echocardiography on a commercially available ultrasound platform (Sequoia C512, Siemens, Mountain View, California) with a 3-5 MHz transducer. The LV end-diastolic dimension, LV systolic dimension, and left atrial dimension were measured by M-mode at parasternal long- and short-axis views. LV ejection fraction was measured using the modified Simpson's method on images of apical 4- and 2-chamber views. Cardiac output was calculated by 2D and Doppler parameters measured at LV outflow tract. Two-dimensional CE was performed with a perfluoropropane gas-filled, lipid-stabilized microbubble, Definity (Bristol-Myers Squibb Medical Imaging, Inc., North Billerica, Massachusetts) as the Echo-enhancing agent; 0.1 to 0.2 ml of Definity was given as a slow intravenous bolus followed by 1 to 3 ml of normal saline flush. Imaging of the contrast agent was performed with a mechanical index of 0.4 to 0.6 and the focal zone positioned in the middle of the LV. The width of the ultrasound scan, imaging depth, and spatial temporal settings were optimized to achieve the highest possible frame rate. All cine data from 3 consecutive cycles were acquired with the acoustic capture technique. Apical 4-chamber and apical long-axis views were acquired to provide the best visualization of the LV vortex formation. The temporal resolution was 16.4 ± 3.5 ms with 60 to 80 frames/cardiac cycle. All stored images were analyzed by 2 blinded independent observers.

Image analysis: particle image velocimetry (PIV)

PIV is an optical method used to measure velocities and related properties in fluids (7). The fluid is seeded with particles, which, for the purposes of PIV, are generally assumed to faithfully follow the flow dynamics. It is the motion of these seeding particles that is used to calculate velocity information (6–8). In our study, analysis was performed with PIV prototype software by Siemens Ultrasound. A hierarchical PIV method that iteratively reduces the interrogation window is adopted and completed with a feature tracking algorithm to handle the long-range correlations due to large velocity values (5,7,9). Although the PIV method was developed for optical flow acquisition, a similar calculation, performed on raw data, was previously shown to be feasible on ultrasound imaging (6). This technique estimates the velocity in an interrogation region of interest (ROI) by determination of the displacement of ROI in the successive frame that produces the maximum similarity between the original and displaced ROIs. The maximum similarity was defined as the value that minimizes the error, in a least square sense, of the transport of brightness: $B(x, y, t)(dB/dt + vx \cdot dB/dx + vy \cdot dB/dy)$ that would be zero in a perfectly rigid motion.

Velocity vectors were evaluated on a regular grid with a spacing of 8 pixels (approximately 2.8 mm). The interrogation window was reduced iteratively by halving its side from squares 32 × 32 up to 8 × 8 pixels. At the first iteration, the 32 × 32 windows in the 2 consecutive frames were placed in the same position, centered at the grid point. In the following

iterations, when the first velocity estimation was performed, the windows were displaced of the length corresponding to velocity value for improving the estimation. Each level of iteration was performed in 2 further substeps, for second order accuracy, where the half of the value of the first estimation was employed to displace the ROIs for the second evaluation. Such computed values are finally smoothed by applying a 3 × 3 Gaussian filter of width equal to the grid distance. Results from 3 consecutive beats were phase-averaged to improve the quality of estimation. This process was defined after an extensive sensitivity study of the many possible parameter values and technical implementation details; this resulted in a combination that ensured robust estimation, that was not significantly influenced by variation of such parameters about these values. The accuracy of velocity values was bounded from below (low velocities) and above (high velocities). Velocity was estimated on the basis of displacement of back scatter (contrast agent bubbles). Therefore, a lower bound on the velocity value was given by displacement of 1 pixel to the next. When the pixel size was 0.33 mm, and the frame rate was 60 Hz, this displacement corresponded to a velocity of approximately 2 cm/s. The upper bound corresponds to the size of the initial interrogation window (here taken as 32 pixels, which means about 60 cm/s).

From the velocity vector, the vorticity, the curl of velocity = $\partial v_x/\partial y - \partial v_y/\partial x$ was computed by second-order accurate finite differences. The PIV data were analyzed frame by frame (Online Video 1), and parametric imaging of the average flow structure was then also extracted. The instantaneous velocity vectors were superimposed on the Doppler color-map showing dominant color paths. The vortex flow pattern can be analyzed frame by frame using this image (Fig. 1A). The velocities were computed on a fixed grid. The pictures show velocity vectors at irregularly spaced points (allowed to move with the flow up to a small distance) for visualization improvement on the video clips where the vectors at such points are obtained (using bilinear interpolation) from the neighboring original grid points. The average flow structure on the heartbeat was obtained by performing Fourier decomposition in time. The first Fourier harmonic (zeroth order) represents the average flow field or the steady streaming contribution to the flow. The second Fourier harmonic (first order) represents the fundamental pulsatile contribution. The steady streaming vorticity field, normalized to the vortex maximum vorticity (color scale from −1 to 1), and the superimposed steady streaming velocity vectors (arrows) together with the steady streaming in-plane streamlines, which represent the location and shape of the vortex, are shown as the average flow pattern (Fig. 1B). The vorticity map allows recognition of the basic flow structure and identification of shear layers (an elongated layer of friction between streams with differential motion), boundary layers (a shear layer next to a wall), and a vortex (a region of compact vorticity). The pulsatile features of the flow, which are the streamlines of the principal harmonics are shown superimposed on the pulsatile vorticity amplitude normalized to the maximum vorticity (color scale from 0 to 1). This represents the strength and pulsatility of the vortex with respect to the average flow (Fig. 1C).

Quantitative vortex flow parameters

For the evaluation of location of vortex, we measured vortex depth (VD) and vortex transversal position (VT). VD represents vertical position of the center of vortex relative to LV long axis (Fig. 2A), and VT represents the transverse position relative to the

posteroseptal axis (Fig. 2B). Vortex length (VL) and width (VW) were measured as the shape of vortex. VL was measured by the longitudinal length of vortex relative to LV length (Fig. 2C), and VW was measured by the horizontal length of vortex relative to LV length (Fig. 2D). A vortex sphericity index (SI) was calculated by VL and VW. Mathematical formulae for the average vortex parameters were described in the Online Appendix.

For the evaluation of pulsatility of LV vortex, we suggested 3 pulsatility parameters including relative strength (RS), vortex relative strength (VRS), and vortex pulsation correlation (VPC) of LV vortex. The RS represents the strength of the pulsatile component of vorticity with respect to the average vorticity in the whole LV. This is simply the ratio between the total vorticity strength of the first order Fourier harmonic and the vortex strength of the zeroth order Fourier harmonic. The first order is the main pulsatile contribution, while the zeroth order is the steady contribution. Thus, this ratio represents the relevance of pulsatility in the LV field (Fig. 3A). The VRS represents the same ratio accounting for the pulsatile vorticity of vortex only instead of the entire LV (Fig. 3B). The VPC is the correlation between steady and pulsatile vorticity in the vortex, normalized with the vortex strength and area to make a dimensionless parameter. It is larger when pulsatility vorticity is located where the steady vorticity is also present. If there was a strong vortex, the pulsatility map showed red color. The details on how to calculate average and pulsatility parameters were described in the Online Appendix.

Two double-blinded examiners repeatedly performed the measurements on 10 randomly selected patients (5 normal and 5 abnormal patients) for intraobserver and interobserver analysis. The second observer repeated the measurements 1 month after the first time. Case sequence was randomly arranged each time.

Statistical analysis

Continuous variables were presented as mean and standard deviation and were compared using the independent Student *t* test. Comparison of categorical variables was made by the chi-square test. Also, the bias tests for intraobserver agreement were compared using paired *t* test. A p value <0.05 was considered statistically significant. All statistical analyses were performed using the SPSS statistical package (SPSS version 13.0, SSPS Inc., Chicago, Illinois).

RESULTS

Clinical data

Clinical characteristics of the study population are shown in Table 1. Mean age was 52 ± 18 years for the control group. Of the 15 patients with abnormal LV function (mean age 55 ± 12 years), 13 (86%) were male patients. There was no significant difference in age and gender between the normal and abnormal LV function groups. The LV ejection fraction (30.1 ± 9.3% vs. 64.4 ± 6.6%, $p < 0.001$) and cardiac output (3.5 ± 1.3 l/min vs. 5.3 ± 1.4 l/min, $p < 0.001$) were significantly lower in the abnormal LV function group. The LV end-diastolic dimension (56.5 ± 9.2 vs. 46.5 ± 7.6, $p < 0.001$), LV systolic dimension (44.8 ±

12.5 vs. 29.0 ± 9.7, p < 0.001), and left atrial dimension (44.9 ± 7.4 vs. 35.6 ± 7.5, p < 0.001) were greater in the abnormal LV systolic function group.

Characterization of LV vortex flow

The time sequence analysis of normal LV flow pattern is shown in Figures 4 and 5 (Online Video 2). During ejection (Figs. 4A to 4C), the direction of the contrast-vector flow was from LV apex to LVOT. After the aortic valve closure, in the early isovolumic relaxation (IVR) period, the direction of flow reversed from LV base to apex with a brief appearance of vortex in the proximity of the mitral valve (Fig. 4D, arrow). During the mid-late IVR period (Figs. 4E and 4F), the nonvertical columnar flow was seen directed from base to apex (Online Video 3). In the early diastolic period (Fig. 5A), an irrotational flow associated with early LV filling dominated the vector representation of flow. In diastasis (Fig. 5B), a relatively apically located vortex was seen (Fig. 5B, arrow). This was followed by a late filling phase of atrial contraction, which was characterized by irrotational flow obscuring the vortex (Fig. 5C, Online Video 4). After mitral valve closure, in the early isovolumic contraction (IVC) period, the vortex was relocated in the proximity of anterior mitral leaflet in the LVOT region (Fig. 5D, arrow) and directed flow from LV apex to LVOT (Fig. 5D). During late IVC period, the vortex persisted in the LVOT region and directed flow towards the aortic valve (Fig. 5E). With the aortic valve opening and ejection (Fig. 5F), the vortex dissipated with continued flow from apex to LVOT. In patients with abnormal LV systolic function (Fig. 6), the vortex was located at the center of the LV throughout diastole and systole and did not redirect flow in a coherent, sequential fashion as in normal subjects (Online Video 5).

Time-averaged flow data and Echo freeze frames in apical long-axis represent the divergence-free velocity vector on the scan-plane, superimposed on the reconstructed Doppler representation (Fig. 7). In normal subjects, the average vortex was compact, elliptically shaped, and was located apically (Fig. 7A, arrow). This vortex was persistent during diastole and directs vectors towards the LVOT (Fig. 7A). In patients with abnormal LV systolic function, a spherical, centrally located vortex was observed with incoherent direction of LV flow (Fig. 7B). In the parametric images shown in the lower panel of Figure 7, the average vortex was a compact and elliptical shaped blue color (SI: 2.8) (Fig. 7Aa). In the abnormal systolic function group, the vortex was of spherical shape (blue color, SI: 1.3) (Fig. 7Ba). The pulsatility of the vortex was stronger (red color area) in normal subjects (Fig. 7Ap) and weaker (blue color) in patients with LV systolic dysfunction (Fig. 7Bp).

Quantitative analysis of LV vortex flow

VD and VL were significantly lower in the abnormal LV systolic function group, compared with that in the normal LV function group (0.443 ± 0.04 vs. 0.482 ± 0.06, p < 0.05; 0.366 ± 0.06 vs. 0.467 ± 0.05, p < 0.01, respectively). VW was greater (0.209 ± 0.05 vs. 0.128 ± 0.06, p < 0.01) and SI was lower (1.86 ± 0.5 vs. 3.66 ± 0.6, p < 0.001) in the abnormal group. RS (1.13 ± 0.4 vs. 2.10 ± 0.8, p < 0.001), VRS (0.57 ± 0.2 vs. 1.19 ± 0.5, p < 0.001), and VPC (0.63 ± 0.2 vs. 1.31 ± 0.5, p < 0.001) were significantly lower in the abnormal group. There was no significant difference in VT between the 2 groups (−0.014 ± 0.05 vs. −0.028 ± 005, p = NS) (Table 2, Fig. 8).

Intraobserver and interobserver analysis

As listed in Table 3, there was no statistically significant difference between the 2 observers or within an observer for quantitative vortex parameters.

DISCUSSION

The present study is the first clinical investigation of the quantitative LV vortex flow using CE. Using the vector PIV and CE, we were able to obtain successfully the quantitative parameters of the intraventricular blood flow vorticity pattern.

LV vortex flow

There has been emerging interest in accurate evaluation of intraventricular vortex, underlying the close relationship between the intraventricular blood flow pattern and the ventricular function (2,3,10–13). During LV filling, the shear layer between the high-speed mitral jet and surrounding still fluid tends inevitably to roll up and accumulate into what is initially the jet head, and eventually becomes the intraventricular vortex (11). Shear flow and vortices dominate the energetic of any flow; this vortex stores part of the kinetic energy of the entering flow into its rotary motion, and redirects toward the outflow track (7). Several studies using MRI have demonstrated that in the LV, inflow through the open mitral valve gives rise to recirculating flows beneath the valve leaflets, the dominant direction being under the free edge of the anterior mitral leaflet (2,4). In addition, it has been reported that anterior vortex is more important than posterior vortex for determining a patient's hemodynamic state (10,11). The past studies of LV flow dynamics using MRI suggest that vortices within the LV reflect the function and geometry of the ventricle, and abnormal vortices may reflect the underlying suboptimal fluid dynamics of dysfunctional LV (2,4). However, there have been no studies using echocardiography to describe the vortex flow parameters in various clinical situations. Kim et al. (2) reported using MR velocity mapping in which anterior vortex developed immediately after the onset of mid-diastolic anterior leaflet closure and reappeared at the time of final mitral valve closure. But a recent study using CE showed vortex flow in the LV was present during the whole diastolic period (14). In our study, the normal control group had a similar vortex flow pattern to that reported in that study. The major anterior vortex developed immediately after the onset of early diastole, and was preserved during the entire diastole. This apparent discrepancy from the previous study could stem from relatively lower temporal resolution of MR (28 ± 3.8 ms) and sensitivity of software used to analyze vortex flow.

CE for the analysis of LV flow vortex

In the human ventricle, Doppler echocardiography and MR velocity mapping have been used to evaluate flow dynamics (4,15). The Doppler method is limited in several ways: 1) the Doppler measures the flow velocity parallel to the scan line, which may not be the principal direction of motion; 2) color Doppler measures the mean velocities and is angle-dependent and thus underestimates the peak velocities; and 3) the frame rate for 2-D color Doppler imaging is lower than that used for contrast imaging. MRI, however, measures velocity distribution, and is limited in temporal resolution, applicability at bedside, a longer test duration, and a higher cost (16,17).

Recent advances in contrast media and ultrasound tissue harmonic imaging techniques have made it possible to visualize and record the movements of single microbubbles in the LV. To this extent, CE may be a better, more convenient modality to investigate the complex flow field in the LV (18,19). The computed velocity field is free of the angle-dependency issue found in Doppler techniques (3,9). Here we extend these observations to a clinical study using a novel vector imaging of CE. We used Definity as the Echo-enhancing agent with low mechanical index. A previous report suggested, through CE-derived PIV, the importance of vortex formation and directed blood flow to optimize LV ejection (14). The PIV technique is noninvasive, and its latest developments allow a high degree of accuracy (5–9). In our study, we were able to achieve good LV vortex flow data using CE with PIV.

In normal subjects, after ejection, the direction of flow reversed toward the apex with a brief appearance of vortex at the early stage of IVR. The major diastolic anterior vortex developed immediately after the onset of the early diastolic phase. This vortex continued during diastasis, and persisted into late LV filling phase. This vortex persisted throughout IVC and dissipated with the opening of the aortic valve and LV ejection. This normal vortex flow sequence is similar to that described in the previous study using CE with PIV in an animal model (14). But, the data from our study have shown that the location and power (pulsatility of the vortex) changed dynamically with the phase of the cardiac cycle. The vortex was relatively apical in diastole and relocated towards anterior mitral valve leaflet in the LVOT region during IVC. However, the vortex is obscured by huge, irrotational, rapidly moving columnar flow from LA to LV in early and late diastole. In our opinion, the role of the vortex in normal subjects changes according to the cardiac cycle. In the IVR period, vortex plays an important role in redirection of flow from base to apex. In early and late diastole, it may prevent collision of rapidly moving flow, enhance reciprocation of atrial and ventricular function, and modulate mitral valve motion. In diastasis, the vortex may serve to preserve the kinetic energy during the relatively static period. In the IVC period, the vortex not only changes direction of flow effectively, but also maintains the kinetic energy until ejection (the aortic valve opening). In patients with abnormal LV systolic function, diastolic vortex was incoherent, persisted at the center of LV during diastole and systole, and was less pulsatile than normal. Also, this vortex did not dissipate even during systolic ejection, potentially accounting for reduced stroke output.

Quantitative LV flow vortex parameters related to LV function

Recent advances in fluid dynamics and PIV provide the technical means to track and quantify the kinematics and velocity field within the LV with the help of low doses of contrast agents (7,9,14). There have been several studies reporting LV flow mechanics in normal patients and those with heart failure using CE (15,16), but no study has reported on quantification of vortex flow parameters related to LV function to our knowledge. In this study, we described several LV vortex parameters responsible for morphological and pulsatile characteristics.

Quantitative parameters related to LV vorticity examined in our study demonstrated that the average vorticity parameters, such as VD, VL, VW, and SI, were significantly reduced in patients with LV dysfunction. The data from our study clearly showed the differences in

quantitative vortex parameters between normal subjects and patients with abnormal LV function. The vortex from the abnormal LV systolic function group was consistently shorter, wider, and rounder than normal. We could quantify not only information about the location and shape of vortex, but also a pulsatility profile of vortex. Pulsatility of LV field and vortex represented by RS, VRS, and VPC were significantly lower in patients with abnormal systolic dysfunction. Therefore, this study illustrates that these quantitative, noninvasive vortex measurements are feasible, reproducible, and distinguishable between normal and abnormal ventricular systolic function. Further, we suggest that quantitative vortex parameters may provide a highly sensitive, novel method to detect early stages of LV dysfunction before gross mechanical changes of LV geometry and function. This remains a matter to be studied further, and we are currently investigating the relationship between changes in the flow parameters and progress of LV dysfunction in more detail.

Clinical implication

The insights into LV vortex flow may have additional and potentially incremental value over the conventional methods to assess LV function. Vortex flow may influence stroke output and efficiency of the LV by redirection of intraventricular flow. This has been explored in a preliminary fashion in previous study (14). Diastolic LV vortex characterization may have implication for diastolic volumetric filling and may provide an index that links diastolic filling to systolic stroke volume (20). There are other potential applications such as association in LV vortex to dyspnea and relationship to symptoms in patients with heart failure.

Study limitations

This clinical study is a pilot study for the LV flow vortex. Limitations of this study include a relatively small number of patients and lack of correlation to an independent reference such as cardiac catheterization or MR contrast study. However, MR is not the gold standard because echocardiography has higher temporal resolution (16.4 ± 3.5 ms with 60 to 80 frames/cardiac cycle) than MRI (28 ± 3.8 ms with 25 to 32 frames/cardiac cycle). Furthermore, our results about qualitative LV vortex analysis are similar to previous studies using MR. But there have been no clinical studies using MR to quantify the vortex flow parameters. The algorithm that we used was unable to detect velocity lower than 1 cm/s. The upper bound corresponds, in principle, to the maximum interrogation window (here taken as 32 pixels, which means about 60 cm/s); in reality, bubbles hardly remain on the scan plane for so long; therefore, high velocities are typically underestimated by this approach. Nevertheless, despite the inaccuracy on low values and limitation on high velocity values, the high density of bubbles allows one to evaluate the flow pattern with high reproducibility, and this attribute is considered here. The approach is also limited to high velocity values principally because of particle migration out of the scan plane. Some particles that are tracked from one frame to the next exit from the plane; however, such particles are not individually detectable because they are present in the same pixel with others. Therefore, the resulting velocity values represent a mixture of the few particles that remain on the scan plane (the higher the velocity, the fewer the particles) and those that leave after a short path, whose velocity is underestimated. These limits cannot be improved by higher frame rate acquisition, but only by a substantial increase of the resolution (reduction of pixel size)

accompanied by a proportionally increased frame rate. Unfortunately, this is beyond the capabilities of the current clinical equipments. However, the narrow error distribution of the large number of sample points indicates that the flow analysis allows evaluation of the flow pattern with high reproducibility when a minimal 3 heart beats were averaged.

The instantaneous velocity values may be affected by noise; to overcome this, we averaged results over 3 heartbeats, and we used a spatial 3 × 3 Gaussian filter (which means that we cannot properly see flow structure of size smaller than approximately 4 mm). In addition, all quantitative results are computed from the steady streaming and first-order time-Fourier harmonic fields that represent averaged result over the entire heartbeat. This quantitative analysis is followed by further averaging of flow fields. They are expressed in dimensionless terms independent of absolute magnitudes. The highest velocity values, whose magnitude cannot be accurately quantified, correspond to “irrotational” parts of the flow (i.e., to bulk nearly uniform flow [like mitral jet core and LVOT]), which do not significantly represent the vortex flow pattern that is made up of moderate-to-low velocity flow. In summary, the averaging process reduces the over 200,000 (per clip) computed velocity values into a few numbers and dramatically reduces the influence of noise; the influence of accuracy located on high velocity values only marginally affects the vortex pattern; the influence of absolute magnitude is reduced by working with dimensionless indicators. Indeed, the processing would even perform better if it could be performed on sector data before scan conversion, but those data are not available to us at the present time. We measured only the component of vorticity normal to the image plane. We recognize that the entire 3-dimensional vortex field, even on the plane, could give better information of the vortex structure, but we had only 2D data and processed 2D image data only. We enrolled only those patients with known advanced LV dysfunction for this initial study. We did not examine patients with mildly impaired systolic function, combined dysfunction of LV systole and diastole, or pure diastolic dysfunction. Vortex parameters of these patient populations will be investigated in future studies.

CONCLUSIONS

The data from this study show that: 1) it is feasible to quantify LV vortex flow using contrast vector profile in normal subjects and those with LV systolic dysfunction; and 2) vorticity imaging by CE using PIV may serve as a novel approach to depict vortex, which is the principal quantity to assess the flow structure. Further confirmatory studies and studies to assess clinical implications are necessary.

Supplementary Material

Refer to Web version on PubMed Central for supplementary material.

Acknowledgments

Dr. Vannan receives research and honorarium support from Siemens and Bristol-Myers Squibb Medical Imaging. Steven Nissen, MD, MACC, served as Guest Editor for this article.

ABBREVIATIONS AND ACRONYMS

2D	two-dimensional
CE	contrast echocardiography
IVC	isovolumic contraction
IVR	isovolumic relaxation
LV	left ventricle/ventricular
LVOT	left ventricular outflow tract
MRI	magnetic resonance imaging
PIV	particle image velocimetry
ROI	region of interest
RS	relative strength
SI	sphericity index
VD	vortex depth
VL	vortex length
VPC	vortex pulsation correlation
VRS	vortex relative strength
VT	vortex transversal position
VW	vortex width

REFERENCES

1. Wu, JZ.; Ma, HY.; Zhou, MD. Vorticity and Vortex Dynamics. Springer-Verlag; Berlin-Heidelberg, Germany: 2006.
2. Kim WY, Walker PG, Pedersen EM, et al. Left ventricular blood flow patterns in normal subjects: a quantitative analysis by three-dimensional mag netic resonance velocity mapping. J Am Coll Cardiol. 1995; 26:224–38. [PubMed: 7797756]
3. Pedrizzetti G, Domenichini F. Nature optimizes the swirling flow in the human left ventricle. Phys Rev Lett. 2005; 95:108101. [PubMed: 16196972]
4. Mohiaddin RH, Yang GZ, Kilner PJ. Visualization of flow by vector analysis of multidirectional cine MR velocity mapping. J Comput Assist Tomogr. 1994; 18:383–92. [PubMed: 8188903]
5. Cenedese A, Del Prete Z, Miozzi M, Querzoli G. A laboratory investigation of the flow in the left ventricle of the human heart with prosthetic, tilting-disk valves. Exp Fluid. 2005; 39:322–35.
6. Kim HB, Hertzberg JR, Shandas R. Development and validation of echo PIV. Exp Fluid. 2004; 36:455–62.
7. Adrian RJ. Particle-image technique for experimental fluid mechanics. Annu Rev Fluid Mech. 1991; 23:261–304.
8. Mukdadi OM, Kim HB, Hertzberg J, Shandas R. Numerical modeling of microbubble backscatter to optimize ultrasound particle image velocimetry imaging. Ultrasonics. 2004; 42:1111–21. [PubMed: 15234173]
9. Domenichini F, Querzoli G, Cenedese A, Pedrizzetti G. Combined experimental and numerical analysis of the flow structure into the left ventricle. J Biomech. 2007; 40:1988–94. [PubMed: 17097665]

10. Kilner PJ, Yang GZ, Wilkes AJ, Mohiaddin RH, Firmin DN, Yacoub MH. Asymmetric redirection of flow through the heart. Nature. 2000; 404:759–61. [PubMed: 10783888]
11. Domenichini F, Pedrizzetti G, Baccani B. Three-dimensional filling flow into a model left ventricle. J Fluid Mech. 2005; 539:179–98.
12. Baccani B, Domenichini F, Pedrizzetti G, Tonti G. Fluid dynamics of the left ventricular filling in dilated cardiomyopathy. J Biomech. 2002; 35:665–71. [PubMed: 11955506]
13. Gharib M, Rambod E, Kheradvar A, Sahn DJ, Dabiri JO. Optimal vortex formation as an index of cardiac health. Proc Natl Acad Sci USA. 2006; 103:6305–8. [PubMed: 16606852]
14. Sengupta PP, Khandheria BK, Korinek J, et al. Left ventricular isovolumic flow sequence during sinus and paced rhythms. J Am Coll Cardiol. 2007; 49:899–908. [PubMed: 17320749]
15. Mizushige K, DeMaria AN, Toyama Y, Morita H, Senda S, Matsuo H. Contrast echocardiography for evaluation of left ventricular flow dynamics using densitometric analysis. Circulation. 1993; 88:588–95. [PubMed: 8339422]
16. Ishizu T, Seo Y, Ishimitsu T, et al. The wake of a large vortex is associated with intraventricular filling delay in impaired left ventricles with a pseudonormalized transmitral flow pattern. Echocardiography. 2006; 23:369–75. [PubMed: 16686618]
17. Shandas R, Gharib M, Sahn DJ. Nature of flow acceleration into a finite-sized orifice: steady and pulsatile flow studies on the flow convergence region using simultaneous ultrasound Dopp ler flow mapping and laser Doppler velocimetry. J Am Coll Cardiol. 1995; 25:1199–212. [PubMed: 7897135]
18. Mulvagh SL, DeMaria AN, Feinstein SB, et al. Contrast echocardiography: current and future applications. J Am Soc Echocardiogr. 2000; 13:331–42. [PubMed: 10756254]
19. Thanigaraj S, Chugh R, Schechtman KB, Lee LV, Wade RL, Perez JE. Defining left ventricular segmental and global function by echocardio-graphic intraventricular contrast flow patterns. Am J Cardiol. 2000; 85:65–8. [PubMed: 11078239]
20. Le Jemtel TH, Alt EU. Are hemodynamic goals viable in tailoring heart failure therapy? Hemodynamic goals are outdated. Circulation. 2006; 113:1027–32. [PubMed: 16493785]

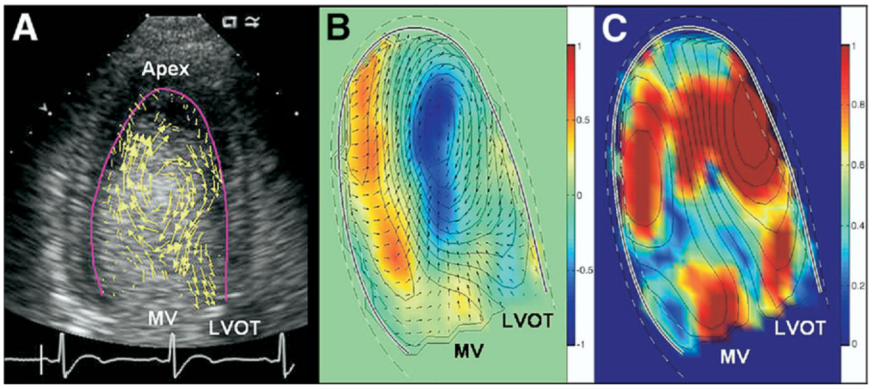

Figure 1. Flow Data by Digital Particle Image Velocimetry From the Apical Long-Axis View

The Echo freeze frames represent the divergence-free velocity vector on the scan-plane, superimposed to the reconstructed Doppler representation **(A)**. Parametric representations of steady streaming field with superimposed velocity vectors **(arrows)** and the steady streaming in-plane streamlines along the divergence-free velocity field **(B)**. The pulsatile strength field with superimposed pulsatile in-plane streamlines **(C)**. LVOT = left ventricular outflow tract; MV = mitral valve. See Online Video 1.

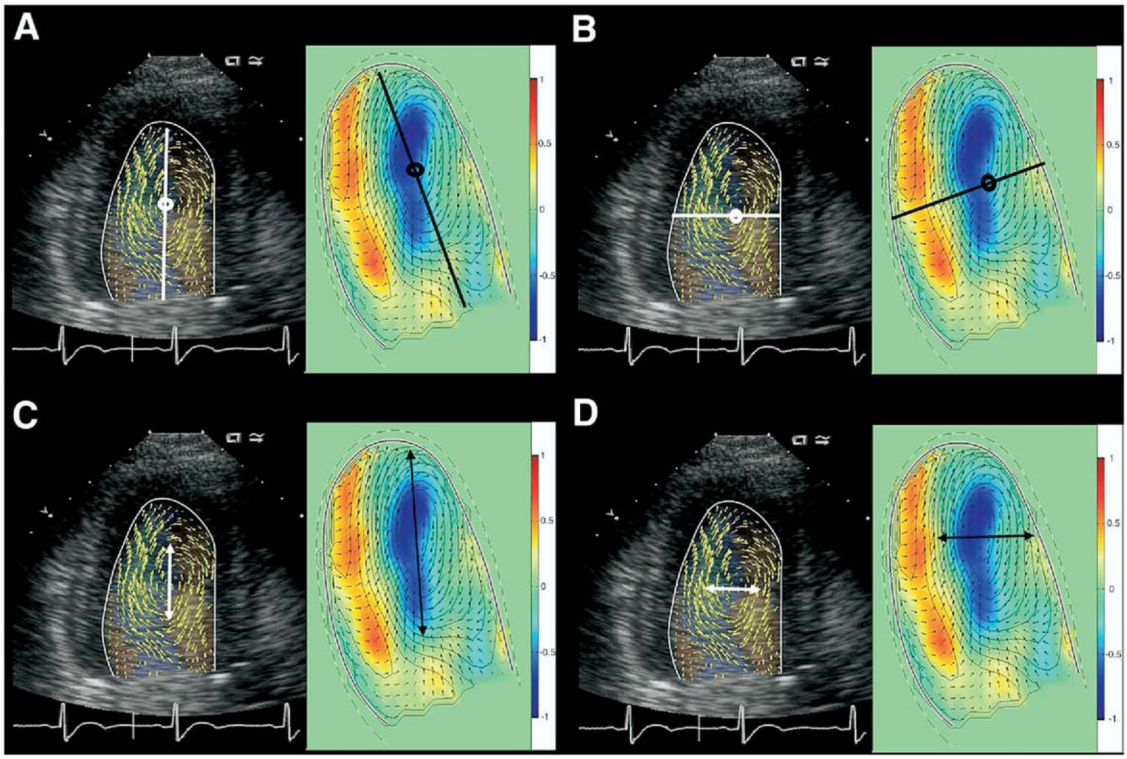

Figure 2. Description of How to Measure Quantitative Average Vortex Parameters That Represent Vortex Location and Shape

Vortex depth represents vertical position of center of vortex relative to left ventricular long axis **(A, white line)**, and vortex transverse position represents transverse position relative to posteroseptal axis **(B, white line)**. Vortex length was measured by longitudinal length of vortex relative to left ventricular length **(C, white arrow)**, and vortex width was measured by horizontal length of vortex relative to left ventricular length **(D, white arrow)**. A vortex sphericity index was calculated by vortex length and vortex width.

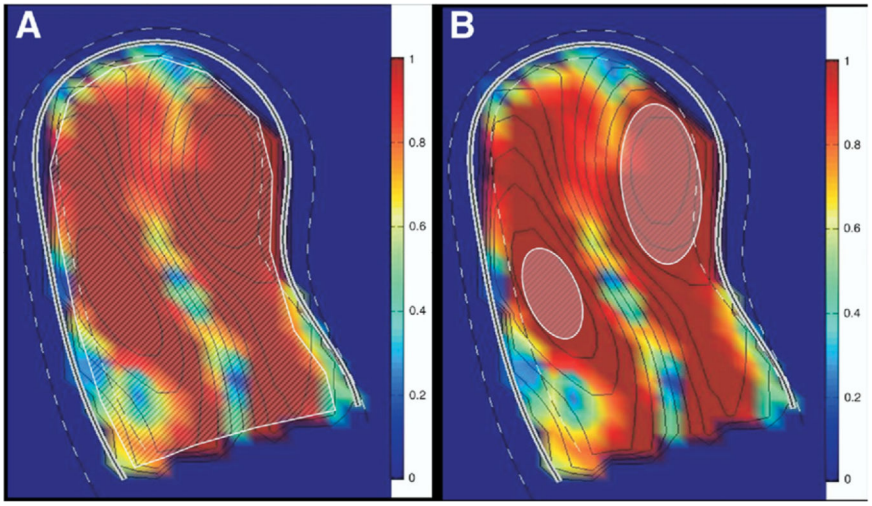

Figure 3. Description of Quantitative Vortex Pulsatility Parameters

The relative strength represents strength of the pulsatile component of vorticity with respect to the average vorticity in the whole left ventricle **(A, white circled area)**. The vortex relative strength represents the strength of the pulsatile vorticity of vortex **(B, white circled area)**.

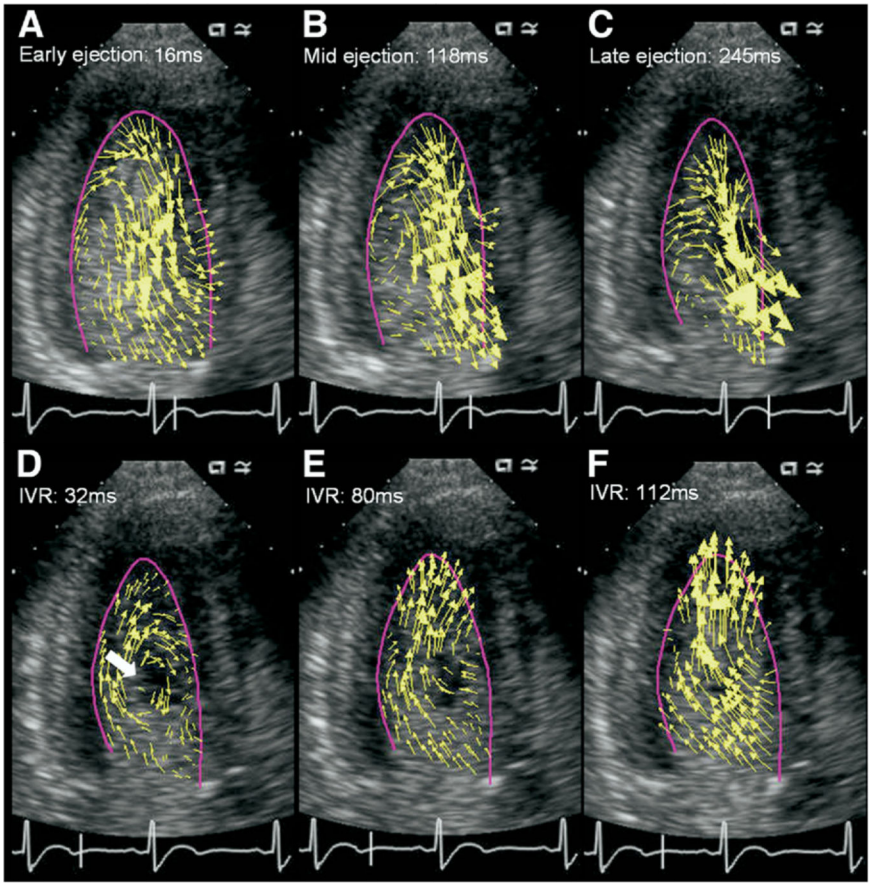

Figure 4. Time Sequence Analysis of LV Flow During Ejection and IVR Period in Normal Subjects

During ejection **(A to C)**, the direction of the contrast-vector flow was from left ventricular (LV) apex to LV outflow tract. After the aortic valve closure, in the early isovolumic relaxation (IVR) period, the direction of flow reversed from LV base to apex. During mid-late IVR period **(E and F),** the nonvertical columnar flow was seen directed from base to apex (early ejection: 16 ms after aortic valve opening **[A]**; mid-ejection: 118 ms after aortic valve opening **[B]**; late ejection: 245 ms after aortic valve opening **[C]**; IVR: 32 ms, 80 ms, and 112 ms after aortic valve closure **[D to F])**. See Online Video 2.

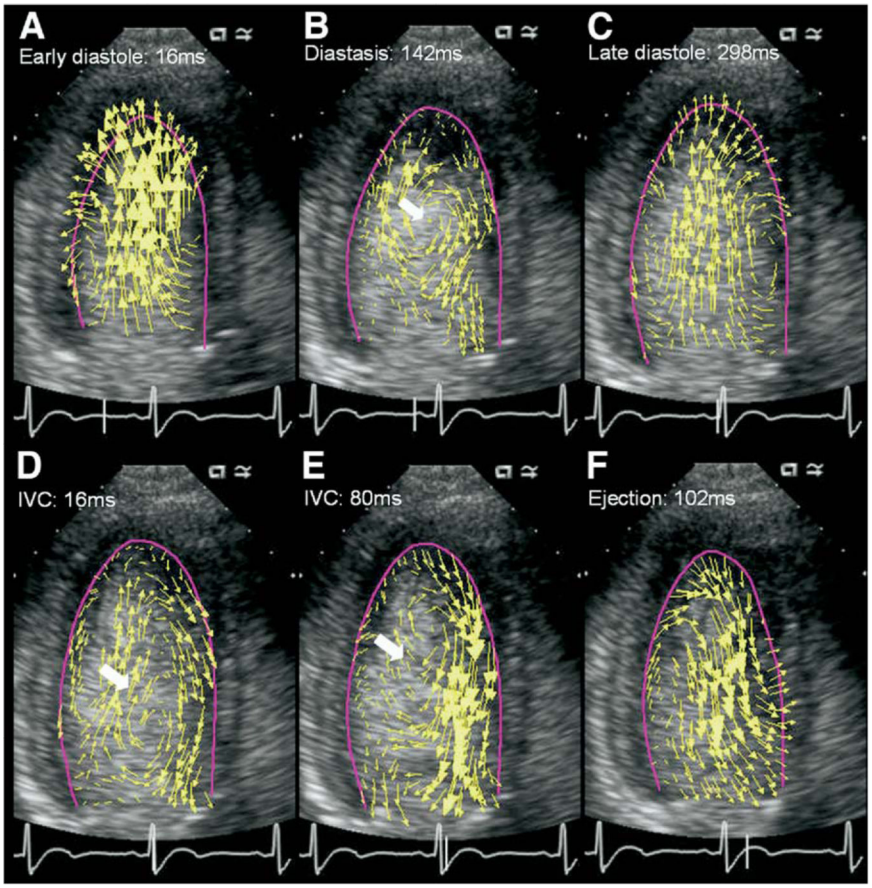

Figure 5. Time Sequence Analysis of LV Flow During Diastole and IVC Period in Normal Subjects

In the early diastolic period **(A)**, an irrotational flow associated with early left ventricular (LV) filling dominated the vector representation of flow. In diastasis, a relatively apically located vortex was seen **(B, arrow)**. This was followed by a late filling phase that was characterized by an irrotational flow obscuring the vortex **(C)**. In the early isovolumic contraction (IVC) period, the vortex was relocated in the proximity of the anterior mitral leaflet in the LVOT region **(D, arrow)**. During the late IVC period, the vortex persisted in the left ventricular outflow tract region and directed flow towards aortic valve **(E)**. With the aortic valve opening and ejection **(F)**, the vortex dissipated with continued flow from apex to left ventricular outflow tract. Early diastole: 16 ms after mitral valve opening **(A)**; diastasis: 142 ms after mitral valve opening **(B)**; late diastole: 298 ms after mitral valve opening **(C)**; IVC-1: 16 ms after mitral valve closure **(D)**; IVC-2: 80 ms after mitral valve closure **(E)**; ejection: 102 ms after mitral valve opening **(F)**. See Online Videos 3 and 4.

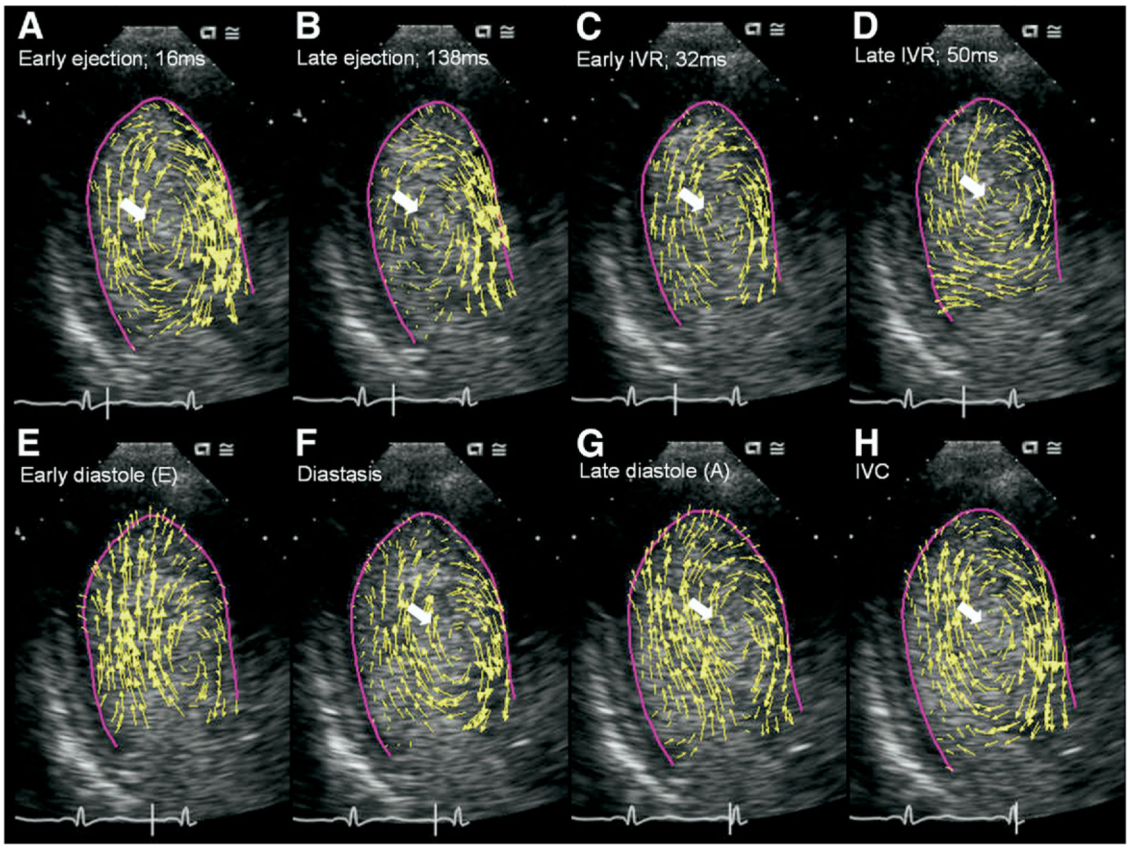

Figure 6. Time Sequence Analysis of LV Flow During 1 Cardiac Cycle in Abnormal LV Systolic Function Group

The vortex was located at the center of the LV throughout diastole and systole and did not redirect flow in a coherent, sequential fashion as in normal subjects. Early ejection: 16 ms after aortic valve opening **(A)**; late ejection: 138 ms after aortic valve opening **(B)**; IVR-1: 32 ms after aortic valve closure **(C)**; IVR-2: 50 ms after aortic valve closure **(D)**; early diastole: 32 ms after mitral valve opening **(E)**; diastasis: 124 ms after mitral valve opening **(F)**; late diastole: 245 ms after mitral valve opening **(G)**; isovolumic contraction period (IVC): 64 ms after mitral valve closure **(H)**. Abbreviations as in Figure 4. See Online Video 5.

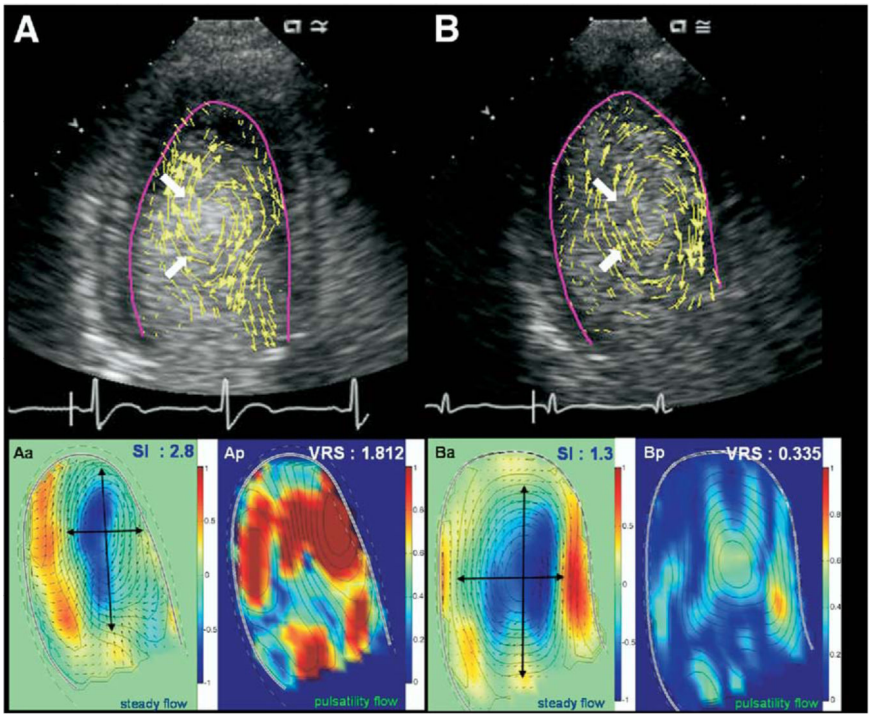

Figure 7. Quantitative Vortex Flow Parameters in Normal Subjects and LV Systolic Dysfunction Group

The Echo freeze frames **(upper panel)**, and parametric representation of steady streaming field and the pulsatile strength field **(lower panel)** in normal **(A)** and left ventricular (LV) systolic dysfunction groups **(B)**. The vortex in normal subjects showed an elliptical shape (**A, Aa, white arrow**, sphericity index [SI]: 2.8) and strong pulsatility (**Ap, red-colored area**, vortex relative strength [VRS]: 1.182), whereas spherical (**B, Ba, white arrow**, SI: 1.3) and weak pulsatility (**Bp, blue-colored area**, VRS: 0.335) vortex was observed in patients with systolic heart failure.

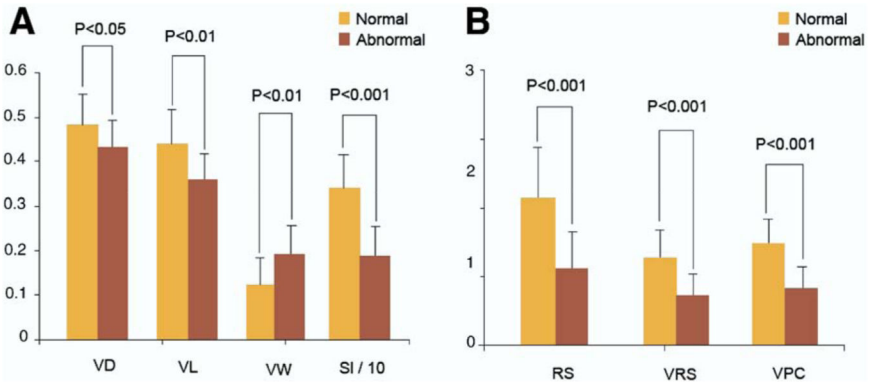

Figure 8. Quantitative Flow Vortex Parameters

Comparison of morphological **(A)** and physiological **(B)** vortex parameters between normal and abnormal LV systolic function group. RS = relative strength; VD = vortex depth; VL = vortex length; VPC = vortex pulsation correlation; VW = vortex width; other abbreviations as in Figure 7.

Table 1

Clinical Characteristics of Patients

Variables	Normal (n = 10)	Abnormal (n = 15)	p Value
Age, yrs	52 ± 18	55 ± 12	NS
Men/women	8/2	13/2	NS
LVDd, mm	46.5 ± 7.6	56.5 ± 9.2	<0.001
LVSd, mm	29.0 ± 9.7	44.8 ± 12.5	<0.001
LAd, mm	35.6 ± 7.5	44.9 ± 7.4	<0.001
LVEF, %	64.4 ± 6.6	30.1 ± 9.3	<0.001
CO, l/min	5.3 ± 1.4	3.5 ± 1.3	<0.001

CO = cardiac output; LAd = left atrial dimension; LVDd = left ventricular diastolic dimension; LVEF = left ventricular ejection fraction; LVSd = left ventricular systolic dimension.

Table 2

Quantitative Vortex Parameters of Normal and Diseased LV

Variables	Normal (n = 10)	Abnormal (n = 15)	p Value
VD	0.482 ± 0.06	0.443 ± 0.04	<0.05
VT	−0.028 ± 0.05	−0.014 ± 0.05	NS
VL	0.467 ± 0.05	0.366 ± 0.06	<0.01
VW	0.128 ± 0.06	0.209 ± 0.05	<0.01
SI	3.66 ± 0.6	1.86 ± 0.5	<0.001
RS	2.10 ± 0.8	1.13 ± 0.4	<0.001
VRS	1.19 ± 0.5	0.57 ± 0.2	<0.001
VPC	1.31 ± 0.5	0.63 ± 0.2	<0.001

RS = relative strength; SI = sphericity index; VD = vortex depth; VL = vortex length; VPC = vortex pulsation correlation; VRS = vortex relative strength; VT = vortex transversal; VW = vortex width.

Table 3

Interobserver and Intraobserver Analysis of Quantitative Vortex Parameter Measurements

	Observer			
Variables	**1**	**2-First**	**2-Second**	**p Value**
VD	0.463 ± 0.04	0.461 ± 0.05	0.459 ± 0.04	>0.05
VT	−0.019 ± 0.03	−0.017 ± 0.04	−0.016 ± 0.04	>0.05
VL	0.397 ± 0.03	0.395 ± 0.03	0.393 ± 0.03	>0.05
VW	0.157 ± 0.02	0.154 ± 0.03	0.153 ± 0.03	>0.05
SI	2.47 ± 0.7	2.49 ± 0.6	2.48 ± 0.5	>0.05
RS	1.63 ± 0.6	1.66 ± 0.5	1.65 ± 0.5	>0.05
VRS	0.82 ± 0.4	0.85 ± 0.4	0.85 ± 0.4	>0.05
VPC	0.87 ± 0.4	0.89 ± 0.3	0.87 ± 0.3	>0.05

Abbreviations as in Table 2.